The Astronomical Journal, 128:829–841, 2004 August

ATLAS VERSUS NEXTGEN MODEL ATMOSPHERES: A COMBINED ANALYSIS OF SYNTHETIC SPECTRAL ENERGY DISTRIBUTIONS

E. Bertone
Instituto Nacional de Astrofísica, Óptica y Electrónica, Luis Enrique Erro 1, 72840 Tonantzintla, Mexico

A. Buzzoni
INAF, Osservatorio Astronomico di Bologna, Via Ranzani 1, 40127 Bologna, Italy

and

M. Chávez[1] and L. H. Rodríguez-Merino
Instituto Nacional de Astrofísica, Óptica y Electrónica, Luis Enrique Erro 1, 72840 Tonantzintla, Mexico
Received 2004 January 28; accepted 2004 May 12

ABSTRACT

We carried out a critical appraisal of the two theoretical models, Kurucz' ATLAS9 and PHOENIX/NextGen, for stellar atmosphere synthesis. Our tests relied on the theoretical fit of spectral energy distributions (SEDs) for a sample of 334 target stars along the whole spectral-type sequence, from the classical optical catalogs of Gunn & Stryker and Jacoby et al. The best-fitting physical parameters ($T_{\rm eff}$, $\log g$) of stars allowed an independent calibration of the temperature and bolometric scale versus empirical classification parameters (i.e., spectral type and MK luminosity class); in addition, the comparison of the synthetic templates from the ATLAS and NextGen grids allowed us to probe the capability of the models to match spectrophotometric properties of real stars and assess the impact of the different input physics. We can sketch the following main conclusions of our analysis: (1) Fitting accuracy of both theoretical libraries drastically degrades at low $T_{\rm eff}$ at which both ATLAS and NextGen models still fail to properly account for the contribution of molecular features in the observed SED of K–M stars. (2) Compared with empirical calibrations, both ATLAS and NextGen fits tend, on average, to predict slightly warmer (by 4%–8%) $T_{\rm eff}$ for both giant and dwarf stars of fixed spectral type, but ATLAS provides, in general, a sensibly better fit (a factor of 2 lower σ of flux residuals) than NextGen. (3) There is a striking tendency of NextGen to label target stars with an effective temperature and surface gravity higher than that of ATLAS. The effect is especially evident for MK I–III objects for which about one in four stars is clearly misclassified by NextGen in $\log g$. This is a consequence of some "degeneracy" in the solution space, partly induced by the different input physics and geometry constraints in the computation of the integrated emerging flux (ATLAS model atmospheres assume standard plane-parallel layers, while NextGen adopts, for low-gravity stars, a spherical-shell geometry). A different $T(\tau)$ vertical structure of stellar atmosphere seems also required for NextGen synthetic SEDs in order to better account for limb-darkening effects in cool stars, as supported by the recent observations of the EROS BLG2000-5 microlensing event.

Key words: stars: atmospheres — stars: fundamental parameters

1. INTRODUCTION

Theoretical computation of model atmospheres has been a leading issue of stellar astrophysics in recent decades. In this framework, Kurucz' (1970, 1979) pioneering work certainly stands as a main reference, together with a few other major contributions like those of Gustafsson et al. (1975) and Tsuji (1976) on the synthesis of red giant stars.

In its more recent versions, Kurucz' (1992a, 1993) ATLAS code included over 58 million spectral lines, providing an accurate description of blanketing effects that modulate ultraviolet emission of stars (Holweger 1970; Gustafsson et al. 1975), and also included nearly all the most important diatomic molecules that shape spectral energy distributions (SEDs) at longer wavelengths. The lack of triatomic molecules (in primis H_2O) and an incomplete treatment of TiO opacity, however, still prevents a satisfactory match to stars cooler than 3500 K (Kurucz 1992b; Castelli et al. 1997). This limit of ATLAS theoretical atmospheres unfortunately affects a number of physical applications dealing, for instance, with the study of cool pulsating variables or the match to the integrated SEDs of galaxies through stellar population synthesis.

More recently, Hauschildt et al. (1999a, 1999b) have presented their PHOENIX/NextGen grid of model atmospheres for dwarf and giant stars. Allard et al. (2000) extended the original bulk of models to the pre–main-sequence (pre-MS) evolution at the low-mass regime. With its 500 million atomic and molecular lines and a spherical geometry treatment of stellar structure, the NextGen library is arguably the most advanced currently available in the literature. As the low-temperature physical regime is suitably sampled, with models as cool as $T_{\rm eff} = 2000$ K, these may possibly fill the gap assuring a homogenous coverage of the stellar fundamental parameters across the whole H-R diagram.

Given the relevance of the Kurucz and Hauschildt et al. contributions, it could be of special interest, at this stage, to carry out a combined analysis of the ATLAS versus NextGen codes in order to check their mutual capabilities in matching spectrophotometric properties of real stars and to assess self-consistency in their input physics. Our analysis follows the Hauschildt et al. (1999a) preliminary discussion and is

[1] Visiting Astronomer at the Steward Observatory and Lunar and Planetary Laboratory, University of Arizona, Tucson, AZ 85721.

carried out in two steps. After a brief description of the main features of each theoretical data set (§ 2), we first try a fit to observations of template stars and compare model outputs (§ 3). This relies on an original optimization procedure, which also provides an estimate of the fit uncertainty across the ($T_{\rm eff}$, $\log g$, [M/H]) phase space. The best fits allow us to establish an effective temperature scale and a calibration of the bolometric correction scale (§ 4). In § 5 we then analyze ATLAS versus NextGen theoretical models for fixed fiducial spectral types. A full summary of the relevant conclusions of our tests is finally given in § 6.

2. INPUT MODEL ATMOSPHERES AND GRID PROPERTIES

ATLAS model atmospheres assume steady-state plane-parallel layers under the hypothesis of local thermodynamic equilibrium (LTE). Line blanketing is computed statistically by means of opacity distribution functions (ODFs), which average the contribution of the different atomic/molecular species through the corresponding oscillator forces (Strom & Kurucz 1966; Kurucz 1970, 1979). For our work, we used the ATLAS 9 version (Kurucz 1993), whose treatment of convection is based on the mixing-length theory (Böhm-Vitense 1958) and accounts for the so-called "approximate overshooting" according to Castelli et al. (1997). The mixing length parameter is set to $\ell/H_p = 1.25$ and the microturbulence velocity to 2 km s^{-1} throughout. The whole theoretical library is made available at the Kurucz web site.[2]

The model library spans a temperature range between $3500 \leq T_{\rm eff} \leq 50,000$ K, sampled at a variable step from 250 to 2500 K with increasing temperature; surface gravity and metallicity cover the interval $0.0 \leq \log g \leq 5.0$ dex in steps of $\Delta \log g = 0.5$ dex, and $-5.0 \leq [{\rm M/H}] \leq +1.0$ dex, respectively. The corresponding SEDs, which also account for line opacity through the ODFs, span from the far-ultraviolet ($\lambda = 90$ Å) to the far-infrared (160 μm), sampled by 1221 wavelength points, with $\Delta\lambda = 10$ Å in the UV and 20 Å in the visual range.

NextGen models have originally been computed by Hauschildt and collaborators with the multipurpose code PHOENIX (e.g., Hauschildt et al. 1996). They assume LTE and plane-parallel geometry for dwarf stars, while a spherical symmetry is adopted in low-gravity model atmospheres ($\log g \leq 3.5$) for giant and pre-MS stars (Hauschildt et al. 1999b; Allard et al. 2000). In striking difference to the Kurucz models, direct opacity sampling is performed including over 500 million lines of atomic and molecular species along the spectrum.

The phase-space domain of the NextGen grid spans the $2000 \leq T_{\rm eff} \leq 10,000$ K range at steps $\Delta T_{\rm eff} = 100$–200 K, with gravity in the interval $0.0 \leq \log g \leq 5.5$ ($\Delta \log g = 0.5$ dex) and metallicity in the range $-4.0 \leq [{\rm M/H}] \leq +0.3$. The SEDs cover the wavelength range from 100 Å to 970 μm, sampled at coarser wavelength steps that can change from model to model (depending on the intervening absorption features in the spectrum). However, a typical $\Delta\lambda = 2$ Å step in the optical region can be picked out. All the data are available via anonymous ftp.[3]

In addition to the standard fundamental parameters (i.e., $T_{\rm eff}$, $\log g$, [M/H]), spherical models in NextGen require one supplementary "dimension" in phase space. As $g \propto M/R^2$ and $L \propto R^2 T^4$, then the emerging luminosity becomes $L \propto (MT^4)/g$. Unlike the plane-parallel case, mean surface brightness therefore depends on the absolute size of stars through the stellar mass (M). Giant-star models in the NextGen grid are computed for 5 $M_\odot$, while pre-MS stars assume 0.1 $M_\odot$. However, mass scaling is found to induce second-order effects in the stellar SED (Hauschildt et al. 1999b), although total luminosity of the models scales, of course, as $L \propto M$ for fixed temperature and gravity.

3. MATCHING SED OF TEMPLATE STARS

A first "sanity" check in our analysis concerns the match with template stars along the whole O → M spectral-type sequence. Comparison with observed SEDs is one of the most natural application of model atmospheres. High-resolution spectra help in investigating the chemical composition of stars, while at lower resolution the shape of the (pseudo) continuum gives clues to the stellar gravity and effective temperature.

3.1. *The Empirical Spectral Libraries*

For our test we considered the complete libraries of stellar spectra by Gunn & Stryker (1983, hereafter GS83) and Jacoby et al. (1984, hereafter JHC84). Both sets of spectra span the whole range of stellar parameters, from giants (MK class I–III) to dwarfs (MK class IV–V), and have been widely used in the literature, particularly for population synthesis studies (e.g., Pickles 1985; Guiderdoni & Rocca-Volmerange 1987; Fanelli et al. 1987; Bruzual & Charlot 1993). The complete sample of target stars amounts to 336 objects (175 stars from GS83 and 161 from JHC84, with no stars in common to the two libraries).

The GS83 data cover a wide wavelength range, from 3130 to 10800 Å, observed at low resolution (FWHM = 20 Å in the blue and 40 Å in the red) and sampled at steps of 10–20 Å. Because of a poorer S/N quality in the ultraviolet, particularly for cool stars (Gunn & Stryker 1983), only the wavelength interval for $\lambda > 3500$ Å is suitable for our analysis. Thanks to better sampling ($\Delta\lambda = 1.4$ Å), the FWHM ~ 4.5 Å resolution of the JHC84 spectra is better exploited, giving a more detailed picture of the main absorption features of template stars in the $3510 \leq \lambda \leq 7427$ Å spectral range. For both the GS83 and JHC84 data sets we had to reject several regions (namely, around 6840–7000, 7140–7350, 7560–7720, 8110–8360, and 8900–9800 Å) affected by telluric bands of O_2 and H_2O.

In our work we adopted the original MK spectral classification by GS83 and JHC84. For 24 out of 26 unclassified objects we relied on the SIMBAD database. All the spectra have been corrected for Galactic reddening and atmospheric extinction as reported in the original data sources.

3.2. *The Theoretical Spectral Libraries*

The subsample of [M/H] = 0 model atmospheres has been used to match the observations. This choice is consistent with the mean metallicity of the GS83 and JHC84 stars. A systematic search from high-resolution abundance studies in the literature actually provided a mean value of

[2] See http://kurucz.harvard.edu.

[3] See ftp://calvin.physast.uga.edu/pub/ and http://dilbert.physast.uga.edu/~yeti. Note that the libraries of dwarf and giant stars available at these sites have lower $T_{\rm eff}$ limits than the published ones.

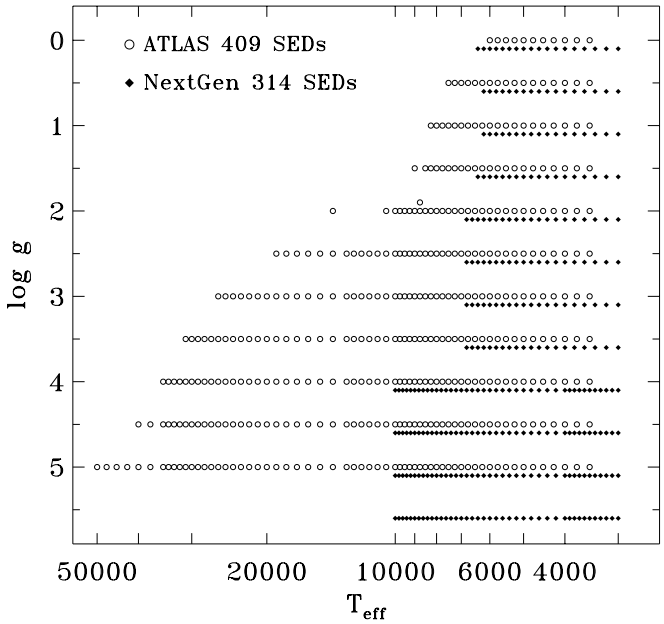

FIG. 1.—Grid of 409 ATLAS and 314 NextGen theoretical models considered in our analysis. A solar metallicity has been assumed throughout.

$[\mathrm{Fe/H}] = -0.10 \pm 0.24$ for 67 stars in the GS83 sample and $[\mathrm{Fe/H}] = -0.06 \pm 0.19$ for 25 JHC84 stars.[4]

A total of 409 theoretical SEDs have been collected from the ATLAS grid, while from the NextGen library we extracted a set of 314 theoretical flux distributions comprising 164 plane-parallel models for dwarfs with $3000 \leq T_{\rm eff} \leq 10,000$ K and $\log g > 3.5$ plus 150 spherical models for giants with $3000 \leq T_{\rm eff} \leq 6800$ K and $\log g \leq 3.5$. The ($T_{\rm eff}$, $\log g$)-space coverage of the two grids is shown in Figure 1.

In order to consistently compare empirical and theoretical libraries, we degraded both GS83 and JHC84 spectra with a Gaussian kernel of FWHM = 25 Å, rebinning the output at constant steps of $\Delta\lambda = 5$ Å. The same procedure has been applied to the ATLAS and NextGen SEDs sampled at the same set of wavelength points. The effect of this low-resolution approach on the results of our analysis (especially on the calibration of the temperature scale) is discussed in some detail in §§ 4 and 5.

3.3. *Fitting Procedure*

A "best fit" for the ($T_{\rm eff}$, $\log g$) fundamental parameters (assuming $[\mathrm{M/H}] = 0$) was searched for each star in the GS83 and JHC84 samples by matching the observed SED with both ATLAS and NextGen libraries. As described in full detail in Bertone (2001) and Bertone & Buzzoni (2001), our method basically relies on a minimization of the statistical variance in the relative flux domain as a measure of the similarity between target spectrum and theoretical SEDs across the reference grid.

Operationally, the spectrum of the ith target star is compared with the jth synthetic SED along the common wavelength range, deriving a residual function

$$X_{(i,j)}(\lambda) = \ln f_i(\lambda) - \ln f_j(\lambda) + k \tag{1}$$

in the flux logarithm domain, as shown in Figure 2. The offset constant, k, in equation (1) is such that

$$\sum_{\lambda} X_{(i,j)}(\lambda) = 0, \tag{2}$$

so

$$k = \left\langle [\ln f_j(\lambda) - \ln f_i(\lambda)] \right\rangle, \tag{3}$$

while the standard deviation

$$s(X)_{(i,j)} = \sqrt{\mathrm{Var}[X(\lambda)]} \tag{4}$$

provides a measure of the spectral likelihood between observations and theoretical models.[5] The underlying hypothesis of our approach is of course that a nondegenerate trend exists for the $s(X)$ function in the ($T_{\rm eff}$, $\log g$) phase space, so that a univocal best solution can be found for a given input SED. For each target star we then mapped the $s(X)$ distribution by matching the whole grid of synthetic model atmospheres and searched for an absolute minimum, $s_{\rm min}$, after performing a cubic spline interpolation of the $s(X)$ points at each gravity. This allowed us to locate the best-fitting values of $T_{\rm eff}$ and $\log g$ with a nominal resolution of $\Delta T_{\rm eff} \sim 10$ K and $\Delta \log g \sim 0.5$ dex, respectively.

Statistical uncertainty of fiducial distinctive parameters was estimated by a one-tail F-test on the value of $s_{\rm min}$ at a 95% confidence level.[6] The $s_{\rm min}$ confidence interval was translated into an equivalent ($\Delta T_{\rm eff}$, $\Delta \log g$) error box relying on a first-order estimate of $\partial s(X)/\partial T_{\rm eff}$ and $\partial s(X)/\partial \log g$ evaluated around the $s_{\rm min}$ region in the phase space. An example of the fitting procedure for a star in the GS83 sample is displayed in Figure 3.

The robustness of our minimization procedure was probed by a bootstrap test. We added a 10% noise to the full set of Kurucz synthetic SEDs and tried our best fit to recover the original (i.e., unperturbed) reference parameters. In all cases, the correct $T_{\rm eff}$ was identified, typically with a 1%–2% uncertainty, a value that was raised to 5%–8% just for the few poorest cases. For surface gravity, the nominal values of the reference models were picked up within ± 0.5 dex in 98% of the cases (i.e., with only eight outliers out of 409 fitted SEDs).

4. TEMPERATURE-SCALE CALIBRATION

Out of the total of 334 stars in the GS83 and JHC84 libraries, a consistent fitting solution for the ($T_{\rm eff}$, $\log g$) fundamental parameters was found for 272 and 230 stars, respectively, using ATLAS and NextGen reference grids. Most

[4] The bulk of metallicity estimates for our star sample comes from the catalogs of Cayrel de Strobel et al. (1997, 2001); other references are Hartkopf & Yoss (1982), Luck (1982), Kjaergaard (1984), Faber et al. (1985), Lambert et al. (1986), Norris (1986), Burkhart & Coupry (1998), Laird et al. (1988), Knude (1989), Luck & Bond (1989), Eggen (1991, 1998), Geisler et al. (1991), Taylor (1991, 1999), Xu (1991), Friel & Janes (1993), Thogersen et al. (1993), Worthey et al. (1994), Bartkevicius & Lazauskaite (1996, 1997), Claria et al. (1996), Zakhozhaj & Shaparenko (1996), Fry & Carney (1997), Flynn & Morell (1997), Schiavon et al. (1997), Takeda & Takada-Hidai (1998), Adelman (1999), Bartasiute et al. (1999), Cenarro et al. (2001), Gray et al. (2001), Haywood (2001), Andrievsky et al. (2002), and Venn et al. (2002), based on different spectroscopic or photometric methods. Note that the only two metal-poor stars (HD 94028 and SAO 102986) in the JHC84 catalog have been excluded in our analysis so that we are eventually left with 334 objects in the GS83 plus JHC84 total sample.

[5] The degrees of freedom for $s(X)$ are settled by the number N of wavelength points after spectrum broadening, as described in § 3.2.

[6] The degrees of freedom of the F distribution, in this case, are simply $N - 1$; see previous footnote.

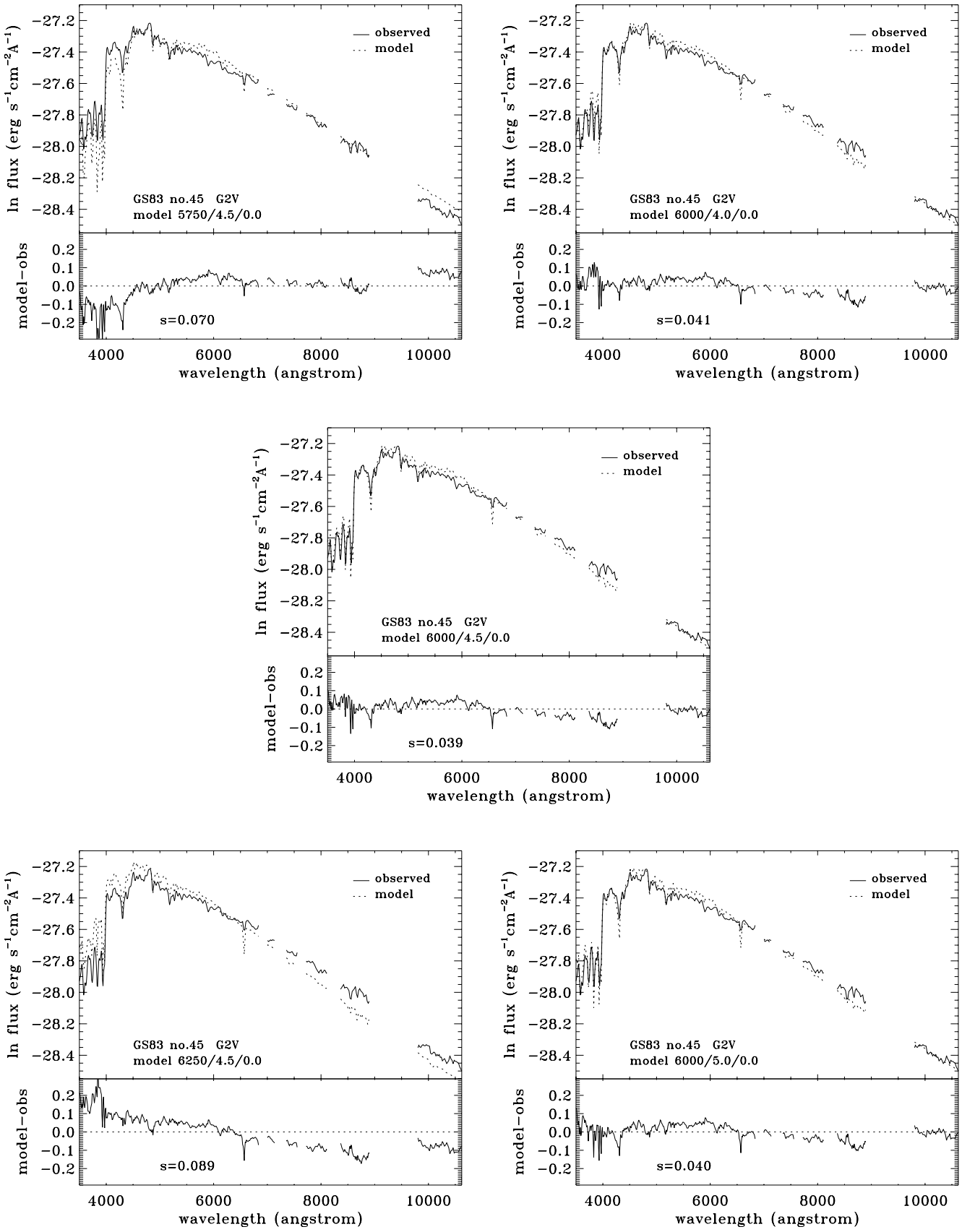

FIG. 2.—Observed SED of star 45 from GS83 (namely, HD 154760, of spectral type G2 V) compared with several ATLAS models. Left plots are for fixed gravity and $\Delta T_{\rm eff} = \pm 250$ K around the reference value of the central panel. Right plots are for fixed $T_{\rm eff}$ and $\Delta \log g = \pm 0.5$ dex. At the bottom of each panel we display the residual function $X_{(i,j)}(\lambda)$ according to eq. (1) with its standard deviation, s, from eq. (4) as labeled. The central panel is the ATLAS best-fit solution for this star.

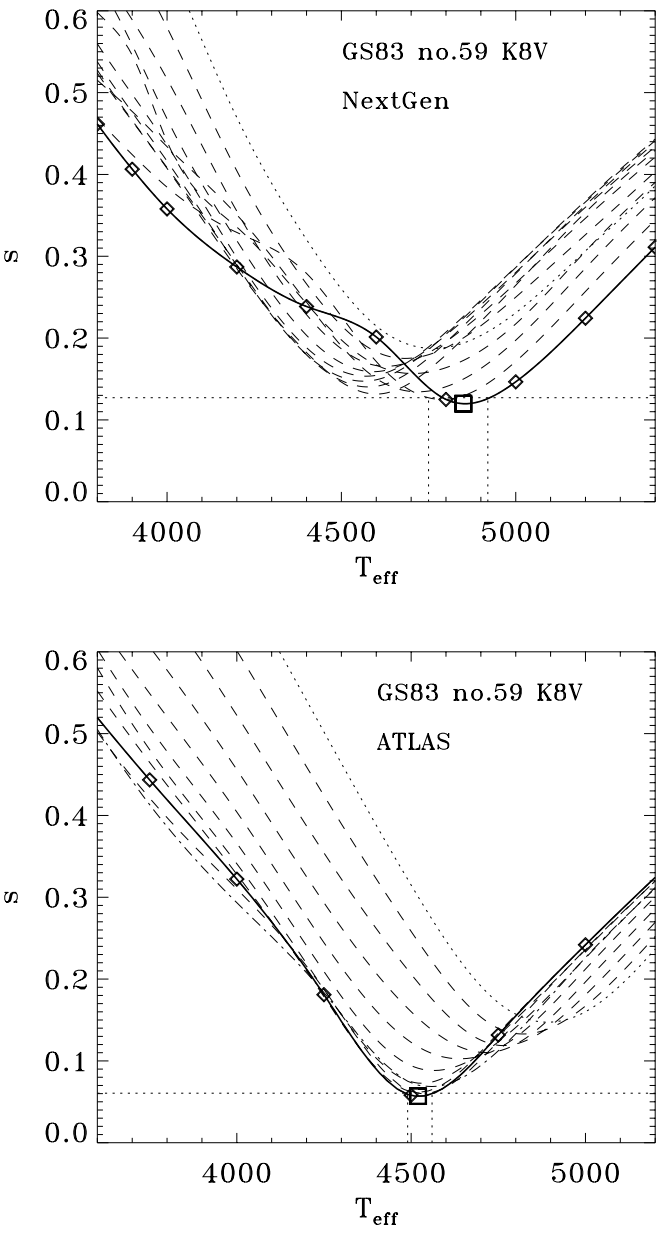

FIG. 3.—Standard deviation of flux residuals for NextGen (*left*) and ATLAS (*right*) fitting models for star BD +38°2457. Each curve connects equigravity points in the grid vs. $T_{\rm eff}$ (*dotted line* for $\log g = 0$, *dash-dotted line* for $\log g_{\rm NG} = 5.5$ or $\log g_{\rm ATLAS} = 5.0$, *dashed* for intermediate values). The solid line is the best-gravity solution with its minimum marked by the big open square. The horizontal dotted line shows the upper limit for $s_{\rm min}$ at a 2 σ confidence level, as resulting from an F statistical test. The fiducial fundamental parameters for this case are $T_{\rm eff} = 4850^{+70}_{-100}$ K, $\log g = 5.5 \pm 0.5$ dex with the NextGen models, and $T_{\rm eff} = 4520^{+40}_{-30}$ K and $\log g = 4.0 \pm 0.5$ dex with the ATLAS models. Note the better accuracy of the ATLAS fit ($s_{\rm min} = 0.06$) compared with NextGen ($s_{\rm min} = 0.12$).

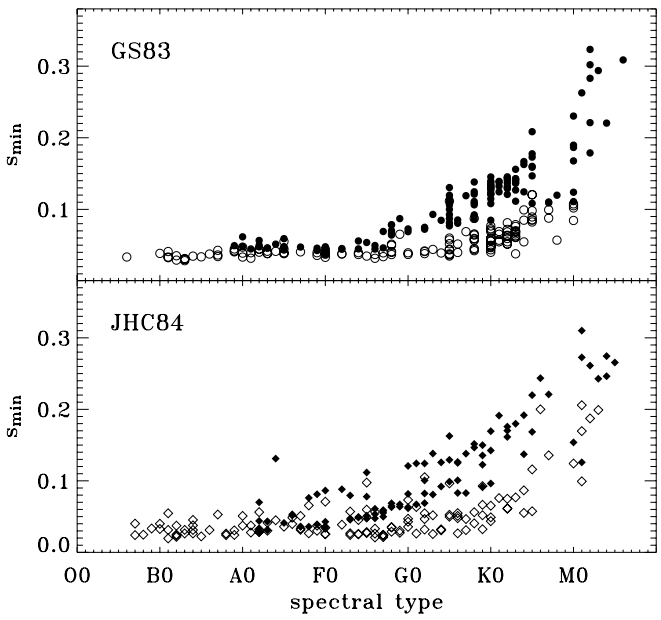

FIG. 4.—$s_{\rm min}$ distribution vs. spectral type for the stars of the GS83 (*top*) and JHC84 atlas (*bottom*). Open markers indicate the results for ATLAS models, filled symbols those from the NextGen grid. Note, for the latter, that a limit at $T_{\rm eff} \leq 10,000$ K does not allow any fit to O–B stars. The value of $s_{\rm min}$ is a measure of the mean percent accuracy of the best fit to the observed spectrum.

of the remaining unfitted objects are M and O–B stars, that is, at the two extreme edges of the temperature scale, for which a fair value for $s_{\rm min}$ cannot be confidently located within the theoretical model grid. The NextGen code, however, has proven to be marginally more efficient in the fit of M stars (of a total of 38 stars in this class, 10 were successfully matched by ATLAS and 24 by NextGen).

The accuracy of the ATLAS and NextGen model libraries in the fit of GS83 and JHC84 stars can be analyzed by means of Figure 4. In the two panels of the figure we report the distribution of the residual standard deviation of the best fits for stars in the two observed samples. As a common feature in the two plots, note that NextGen provides in general a poorer fit compared to the ATLAS code. This is particularly evident for G and K stars ($T_{\rm eff} \sim 5500 \rightarrow 4000$ K), for which ATLAS is a factor of 2 better than NextGen in terms of best-fitting variance. The figure also shows that the accuracy in the definition of the temperature scale directly depends on the wavelength baseline of the spectra. Compared with the GS83 stars, in fact the JHC84 fits are slightly poorer, given a narrower spectral range for the JHC84 library (i.e., $\Delta\lambda \sim 4000$ Å vs. 7500 Å for GS83).

The incomplete treatment of molecular opacity in the Kurucz code is well evidenced in both plots of Figure 4, in the sharp increase of standard deviation in the fit of late-K and M stars. The same problem also seems to affect at a similar level the NextGen fits, confirming in any case a still unsolved and pervasive deficiency of the theory in self-consistently reproducing cool stars.

The temperature scale resulting from the ATLAS and NextGen fits is displayed in Figure 5. We compared with a number of empirical mean loci for dwarfs and giants, including the Johnson (1966) classical compilation and the Böhm-Vitense (1981) scales for hot stars. We also considered the recent calibration of F0–K5 giant stars from Alonso et al. (1999) and the extension to late-M giants of Perrin et al. (1998), which includes the Ridgway et al. (1980) data. Furthermore, Di Benedetto (1998) provided accurate and systematic measures of the effective temperature for a wide sample of 537 stars of A to K spectral type, within an internal accuracy of ±1% in the individual $T_{\rm eff}$ estimates, using the surface brightness technique (Wesselink 1969) calibrated by the angular diameters of 22 stars. His mean locus for the dwarf and giant subsamples is superposed on our data in Figure 5.

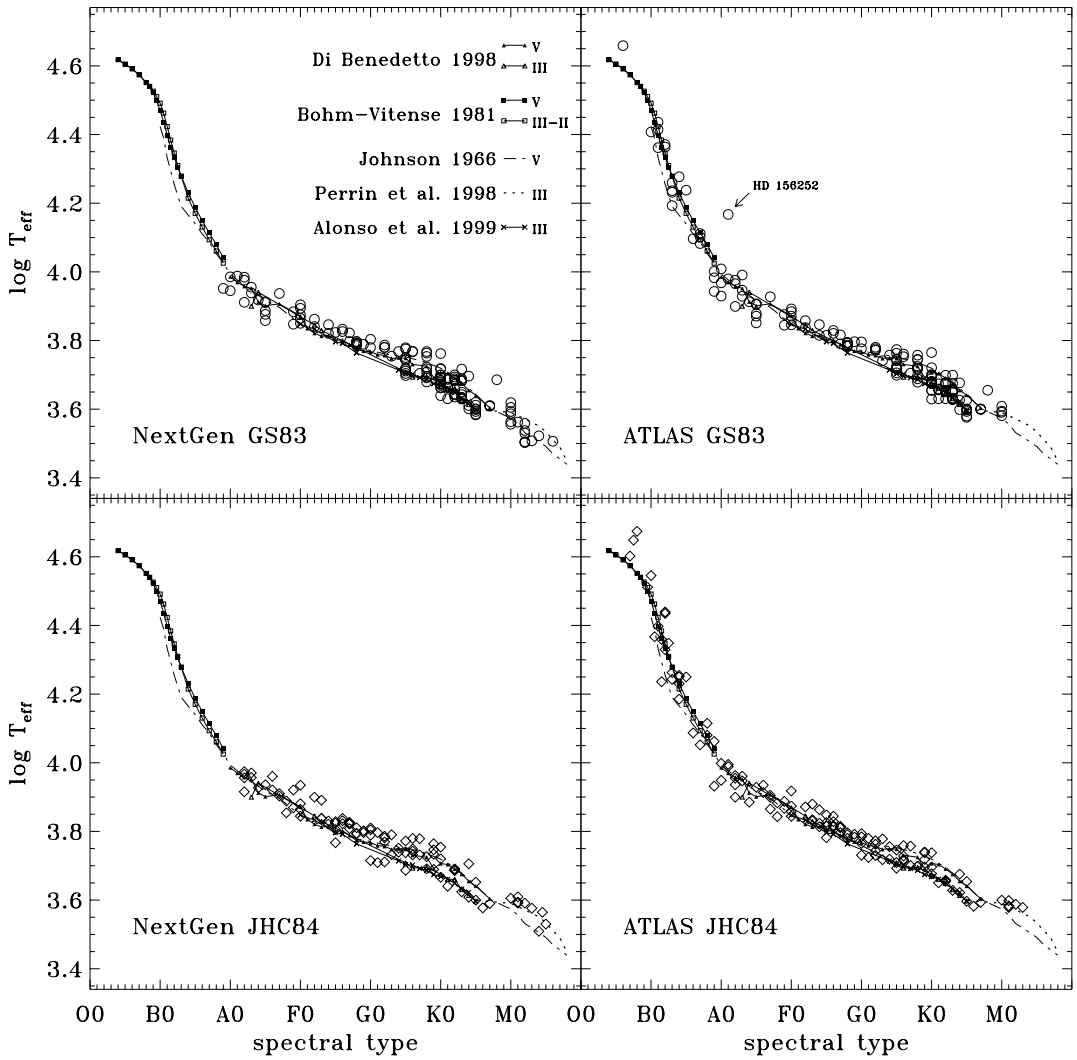

FIG. 5.—Effective temperature scale as derived from the GS83 (*top; circles*) and JHC84 stars (*bottom; squares*), after NextGen (*left*) and ATLAS (*right*) fits. Our results are compared with several empirical calibrations from the literature, as indicated in the top left panel. The outlier star HD 156252 is indicated in the top right panel (note that this object is not in the NextGen plots because of an upper limit to effective temperature of the model grid at $T_{\rm eff} \leq 10,000$ K). See text for discussion.

In general, we find a consistent trend between the $T_{\rm eff}$ scale from the theoretical fits of the GS83 and JHC84 stars and the empirical reference calibrations. The more scattered distribution of our points derives, of course, from the fact that these are fits of individual stars, instead of a mean locus, and from the luminosity and metallicity spread of the sample. Only one clear outlier appears among the GS83 stars in the top right panel of Figure 5, HD 156252 (alias 38 Oph), classified by GS83 as a type A1 V star with (dereddened) $(B-V) = -0.14$ mag and color excess $E(B-V) = 0.16$ mag. The exceedingly blue color calls for a warmer fitting temperature ($T_{\rm eff} \sim 14,000$ K) with ATLAS, while the NextGen match also suggests a temperature in excess of 10,000 K, as no minima of the standard deviation s (see eq. [4]) were present below that temperature.

This star is reportedly among the most reddened ones in the GS83 list but if one accounts, alternatively, for a much lower color excess as reported in the *Hipparcos* catalog [namely, $E(B-V) = 0.015$ mag], then the evident discrepancy between fitting temperature and spectral type could easily be recovered.

To better single out the differences between the NextGen and ATLAS fits, in Figures 6 and 7 we considered separately the main sequence (MK class V) and giant (MK III) star subsamples displaying the $\Delta T_{\rm eff}/T_{\rm eff}$ between our fitting temperature and the reference calibration of Böhm-Vitense (1981) and Johnson (1966) for dwarfs, and Alonso et al. (1999) and Perrin et al. (1998) for giants. Figure 6 shows that both ATLAS and NextGen grids tend to fit F to M stars with a 4%–8% warmer effective temperature, the $T_{\rm eff}$ excess being in general higher for the NextGen fits.

The situation is somehow different for giants (see Fig. 7) with a drift in the point distribution with respect to the Alonso et al. (1999) and Perrin et al. (1998) $T_{\rm eff}$ calibration (but, again, with the NextGen output marginally warmer than the ATLAS one).

As for the Kurucz models, a glance at Figure 2 makes clear that part of the bias toward higher fitting temperatures might derive from the blanketing effects in the ultraviolet region of the stellar SED shortward of 4000 Å. The residual scatter in this spectral region is, in fact, a major source to the global variance when matching observed SED and theoretical

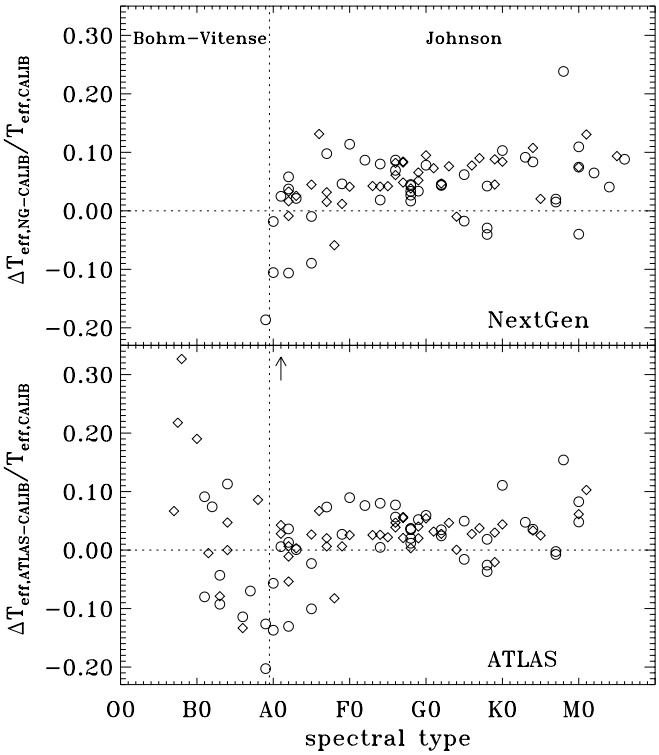

FIG. 6.—The $T_{\rm eff}$ residuals vs. spectral type of ATLAS and NextGen best fits for the subsample of MK V stars and the corresponding calibration of Johnson (1966) for A–M stars and Böhm-Vitense (1981) for O–B-types. Open circles identify GS83 objects, while squares mark the JHC84 stars. The outlier HD 156252 is off the ATLAS plot, as indicated by the vertical arrow (see text for discussion).

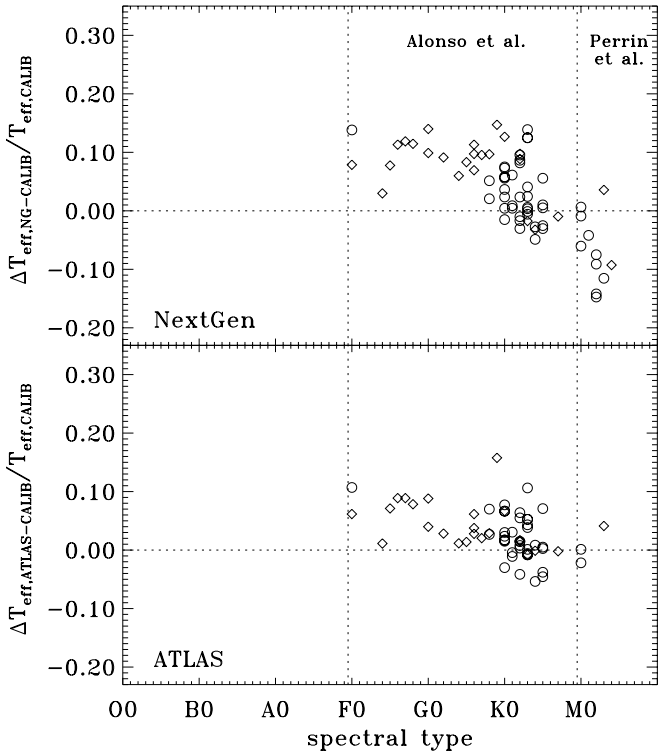

FIG. 7.—Like Fig. 6, but for MK III giant stars vs. the corresponding calibrations of Alonso et al. (1999) for F–K stars and Perrin et al. (1998) for M-type stars.

models, thus sensibly constraining the choice of the best-fit solution. More entangled is the situation for NextGen models, which adopt a different chemical mix representative of solar metallicity. While ATLAS relies on the Anders & Grevesse (1989) solar abundances, NextGen assumes the revised values from Jaschek & Jaschek (1995); for $Z = Z_{\odot}$, this makes NextGen Fe abundances slightly lower compared to ATLAS (namely, $[{\rm Fe_{NG}/Fe_{ATLAS}}] \simeq -0.17$ dex). However, this feature could hardly explain the observed trend in the $T_{\rm eff}$ calibration as a Fe-poorer model atmosphere should actually display a *lower* blanketing, thus allowing a *cooler* temperature to fit the observed SED of stars (see the quantitative discussion by Buzzoni et al. 2001).[7]

4.1. *Bolometric Corrections*

Our best-fitting procedure with model atmospheres allows, in principle, a straightforward estimate of bolometric luminosity for stars in the GS83 and JHC84 samples. When coupled with the individual V magnitudes, this could eventually supply a measure of the bolometric correction (BC).

In order to set the BC scale, for our calculations we identified the theoretical template for the Sun as the ATLAS model SUNK94, with $T_{\rm eff} = 5777$ K, $\log g = 4.44$, and $[{\rm M/H}] = 0.0$ according to Castelli et al. (1997). Its theoretical SED has been convolved with the V filter profile of Bessell (1990) and photometric zero points were set so as to have ${\rm BC}_{\odot} = {\rm Bol}_{\odot} - V_{\odot} = -0.07$ (Bessell et al. 1998).

The BC for each star in the GS83 and JHC84 samples is then computed as

$$\mathrm{BC} = -2.5 \log (\sigma T_{\rm eff}^4) - V - k + 2.22. \qquad (5)$$

Note that in equation (5), the V magnitude derives from the convolution of the *observed* spectrum while the offset k (that properly scales the bolometric magnitude of the theoretical fitting SED) is from equation (3).

Our results are compared in Figure 8 with other standard calibrations for dwarf and giant stars versus. spectral type. We considered in particular the work of Flower (1977) and Johnson (1966) and the later revisions of Bessell (1991) (for late-K and M dwarf stars) and Code et al. (1976) (for hot O–B stars). When necessary, bolometric scales were consistently shifted to assure ${\rm BC}_{\odot} = -0.07$.

The final reference calibration for $T_{\rm eff}$ and BC versus spectral type for dwarf and giant stars according to ATLAS and NextGen is summarized in Table 1. Given the limited spectral coverage of the observed spectra, our bolometric extrapolation suffers, of course, from intrinsic uncertainties at the two extreme edges of the temperature scale, at which a substantial fraction of stellar energy is emitted outside the optical range. The BC calibration of Table 1 for B and M stars should therefore be taken with some caution since it critically relies on the theoretical input physics.

A more extensive discussion of this issue from a fully theoretical point of view has been carried out by Bessell et al. (1998) based on the ATLAS and NMARCS model predictions, the latter from the calibrations of Plez et al. (1992)

[7] As a cross-check in this regard, we tried a fit of the GS83 stars relying on the Kurucz library with $[{\rm Fe/H}] = -0.1$ instead of solar. From the operational point of view, this should roughly mimic the NextGen solar case. As expected, the GS83 fitting temperatures are, on average, 50–100 K cooler than the values obtained with the ATLAS library at $[{\rm Fe/H}] = 0$.

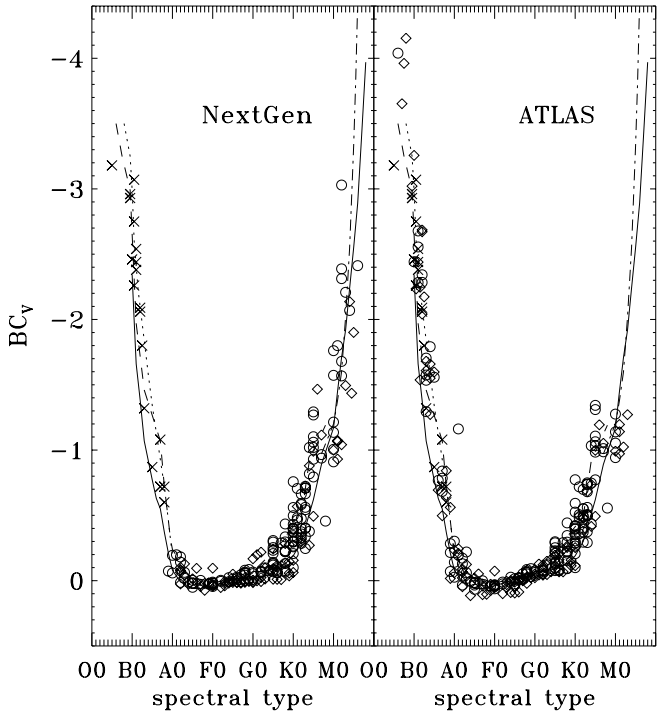

FIG. 8.—Derived bolometric correction for GS83 (*open circles*) and JHC84 (*squares*) stars according to ATLAS and NextGen model atmospheres. Our results are compared with the empirical calibrations of Flower (1977, *dotted line* for MS stars, *dashed line* for giants), Johnson (1966, *solid line*), Bessell (1991, *dash-dotted line*), and Code et al. (1976, *crosses*).

for giants and Edvardsson et al. (1993) for dwarfs. A comparison of our results with those of Bessell et al. (1998) is shown in Figure 9 confirming, however, general agreement with our output.

5. COMPARING TEMPLATE SED ALONG THE SPECTRAL-TYPE SEQUENCE

The whole set of synthetic templates for the GS83 and JHC84 stars prompts a straightforward comparison of the ATLAS versus NextGen code performances, taking into account in a self-consistent way the effect of the different input physics on the match to SEDs for real stars along the O → M spectral-type sequence. For our test we especially relied on the subset of 216 objects from the GS83 and JHC84 catalogs for which a nominally best fit exists both for the ATLAS and NextGen grids over the temperature range $3500 \leq T_{\rm eff} \leq 10,000$ K.

An interesting feature, when comparing the two sets of theoretical templates, as in Figure 10, concerns the distribution of the fitting gravity. It is evident from the histogram that for an important fraction of target stars NextGen tends to fit a higher gravity than ATLAS. This actually led to a number of "catastrophic outliers" among the giant and supergiant stars in the GS83 and JHC84 samples, as shown in Figure 11. In the NextGen plot, in fact, (*top*) 23 out of the 100 MK I–III stars are unexpectedly located in the high-gravity region of the diagram, pertinent to class V dwarfs, with a nominal "best-fit" gravity of $\log g = 5.5$ dex. Conversely, only four such gravity outliers are present in the ATLAS diagram (*bottom*) with a gravity of $\log g = 5$ dex.

A similar trend can also be recognized for the fitting stellar temperature $T_{\rm eff}$, as we discussed in § 4. Again, Figure 12 shows that NextGen $T_{\rm eff}$ estimates are, on average, 2% higher than the ATLAS best-fit values, with a sensibly higher scatter for the JHC84 stars (see bottom panel in the figure), which partly depends on the shorter wavelength baseline compared to the GS83 set of spectra [$\sigma(\Delta T_{\rm eff}/T_{\rm eff}) = 0.031$ dex for the JHC84 sample versus a value of 0.018 dex for the GS83 stars].

The tendency of NextGen to overestimate temperature and gravity can be illustrated by Figure 13, in which we map the distribution of the fit variance (s) across the theoretical grid for two MK III giants in the GS83 and JHC84 samples.[8] One sees from the plots that actually *two* physically distinct solutions exist for these stars, one that correctly locates both K2 III giants in the low-temperature low-gravity range [namely, $(T_{\rm eff},\ \log g) \sim (4500\ {\rm K}, 3.0$ dex) in our example] and adopts a spherical model (i.e., in the $\log g \leq 3.5$ domain) and the other (*nominally better*) one that assumes a plane-parallel geometry but places stars at a much higher $\log g \sim 5.5$ dex and $T_{\rm eff} \sim 4800$ K. This apparent "bimodality" in the solution space is also obvious in the JHC84 panel of Figure 12, in which the giant star distribution appears to split in two distinct sequences depending on whether the spherical or the plane-parallel solution prevails as a best fit.[9]

Note, by the way, that some correlation in the temperature and gravity excess, when fitting empirical SED with theoretical models, can naturally be expected on the basis of the arguments pointed out by Buzzoni et al. (2001). Their experiments showed in fact that a correspondingly higher gravity should likely be required to recover, at medium-high resolution, "too shallow" absorption features predicted by a too warmer model forced to match the low-resolution SED of a given star. According to Buzzoni et al. (2001), such a tight dependence between $\Delta \log T_{\rm eff}$ and $\Delta \log g$ can be written in the form

$$\frac{\Delta \log g}{\Delta \log T_{\rm eff}} = 3000 \left(\frac{1000}{T_{\rm eff}} \right)^3 \ {\rm dex\ K^{-1}}. \qquad (6)$$

A consistent trend in this sense is confirmed in Figure 14, which reports the temperature and gravity differences between ATLAS and NextGen fiducial solutions for the 216 target stars in common.

5.1. *Sphericity Effects on Theoretical SEDs*

Such different behavior seen in ATLAS and NextGen model output calls, of course, for a distinct physical approach in the calculation of the inner structure of the stellar atmosphere. This is especially true for giant stars for which the plane-parallel model atmospheres of ATLAS are compared with the spherical-shell geometry of NextGen. The impact of geometry on the emerging flux of the theoretical models was first assessed in a pioneering work by Scholz & Tsuji (1984) on the atmospheres of M and C stars and more extensively explored in recent years by Plez and collaborators (Plez 1990; Plez et al. 1992).

Basically two intervening effects modulate the integrated SED of spherical models with respect to their corresponding plane-parallel cases. First, as a general trend for fixed $T_{\rm eff}$ and $\log g$, spherical model atmospheres tend to display a lower

[8] This plot is basically a projected view of the three-dimensional fitting surface, like that shown in Fig. 3.

[9] The same effect is not equally evident in the GS83 plot because of the dominant fraction of dwarf stars in this sample.

TABLE 1

Fiducial ATLAS and NextGen Calibration for Temperature Scale and Bolometric Correction

	ATLAS				NextGen			
	Dwarfs		Giants		Dwarfs		Giants	
Spectral Type	$T_{\rm eff}$	BC	$T_{\rm eff}$	BC	$T_{\rm eff}$	BC	$T_{\rm eff}$	BC
B0	30430	−2.99	28640	...	...	...	...	...
B1	25830	−2.56	24910	−2.39	...	...	...	...
B2	22000	−2.14	22020	−2.11	...	...	...	...
B3	18920	−1.75	19470	−1.84	...	...	...	...
B4	16490	−1.41	17230	−1.56	...	...	...	...
B5	...	...	15310	−1.27	...	...	...	...
B6	13090	−0.85	...	...	...	...	...	...
B7	11940	−0.64	12330	−0.74	...	...	...	...
B8	11040	−0.47	11230	−0.52	...	...	...	...
B9	10330	−0.31	10340	−0.33	...	...	...	...
A0	9780	−0.19	9640	−0.18	9730	−0.10	...	...
A2	8980	−0.07	8700	0.00	9030	−0.07	9200	−0.02
A3	8680	−0.03	8400	0.04	8740	−0.03	8930	0.00
A5	8200	0.02	8050	0.06	8300	0.02	8530	0.02
A7	7810	0.03	7880	0.05	7910	0.04	...	...
F0	7290	0.05	7660	0.04	7380	0.04	7810	0.04
F2	6980	0.05	7410	0.05	7080	0.03	7470	0.05
F5	6570	0.02	6830	0.07	6680	0.02	6730	0.03
F7	6330	0.01	6360	0.05	6450	0.02	6350	−0.00
G0	6030	−0.04	5720	−0.03	6140	−0.01	5850	−0.05
G2	5860	−0.08	5420	−0.10	5950	−0.03	5620	−0.07
G5	5590	−0.14	5160	−0.18	5670	−0.08	5410	−0.08
G7	5400	−0.17	5070	−0.22	5490	−0.14	5250	−0.11
K0	5060	−0.24	4850	−0.30	5190	−0.23	4870	−0.27
K2	4820	−0.33	4540	−0.49	4980	−0.33	4550	−0.47
K5	4480	−0.52	3960	−0.98	4630	−0.52	4090	−0.90
K7	4290	−0.71	3720	−1.25	4380	−0.70	3860	−1.17
M0	4010	−0.97	...	...	3990	−1.05	3670	−1.51
M1	3890	−1.04	...	...	3860	−1.19	3630	−1.61
M2	...	...	...	...	3720	−1.37	3550	−1.74
M3	...	...	...	...	...	...	3420	−1.94
M4	...	...	...	...	3450	−1.77	3180	−2.26
M5	...	...	...	...	3320	−2.02	...	...
M6	...	...	...	...	3190	−2.32	...	...

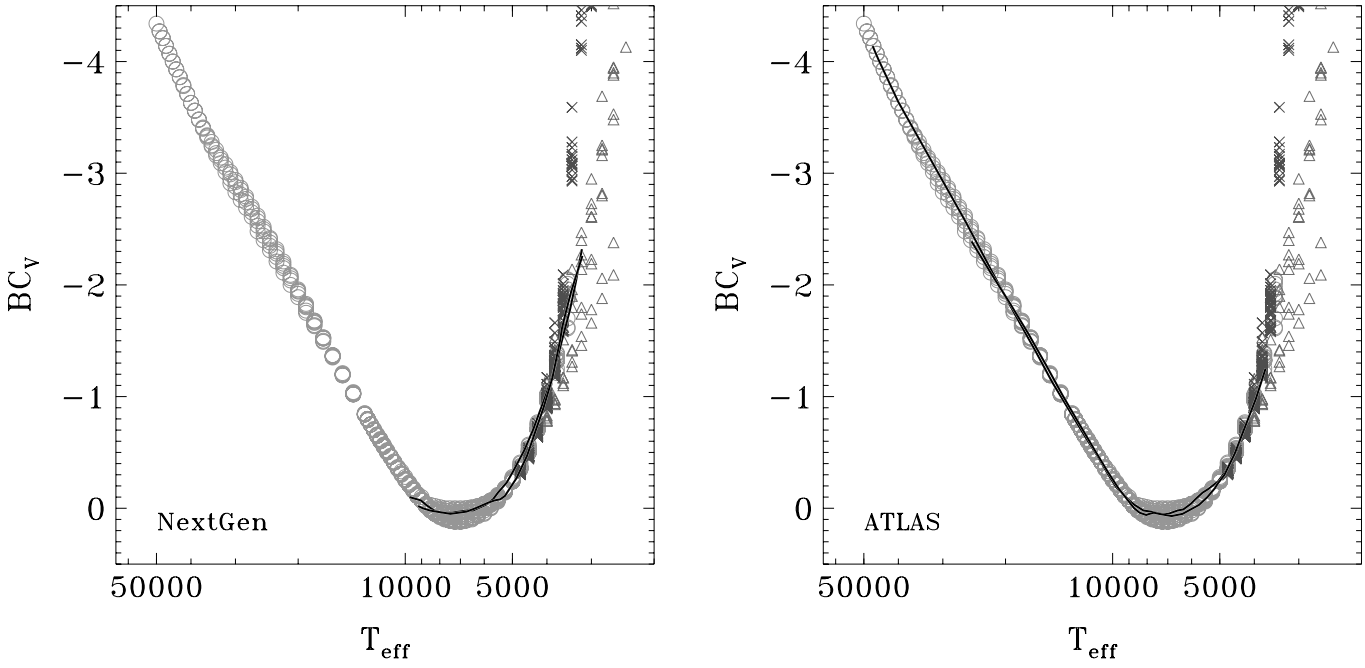

Fig. 9.—Like Fig. 8, but vs. temperature scale for several theoretical calibrations. Our results from Table 1 (*solid lines*) are compared with those of Bessell et al. (1998), also based on the ATLAS models (*open circles*), Plez et al. (1992) for cool giant models (*crosses*), and Edvardsson et al. (1993) for M dwarfs (*triangles*), both relying on the NMARCS atmosphere code of Gustafsson et al. (2003). The left panel reports our NextGen calibration, while the right panel is for the ATLAS theoretical locus.

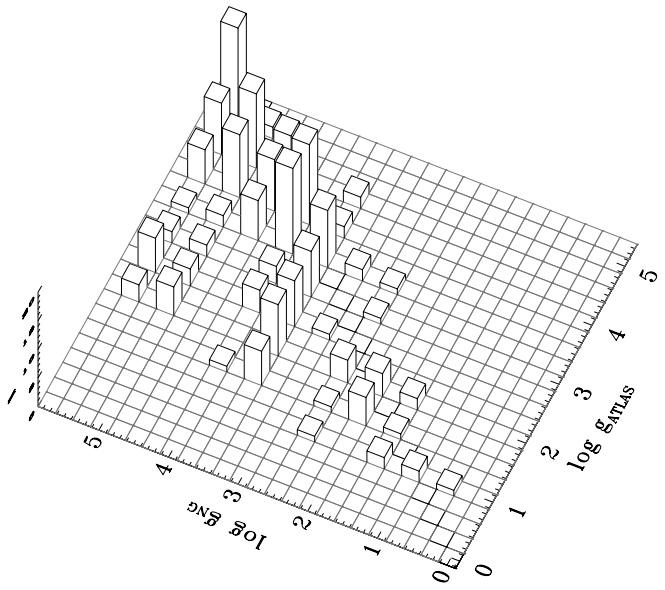

FIG. 10.—The $\log g_{\rm NG}$ vs. $\log g_{\rm ATLAS}$ distribution for the sample of 216 stars with common fitting solutions. The vertical axis shows the frequency number. Note the excess of high-gravity best-fit solutions for NextGen, compared to the corresponding ATLAS distribution (see text for full discussion).

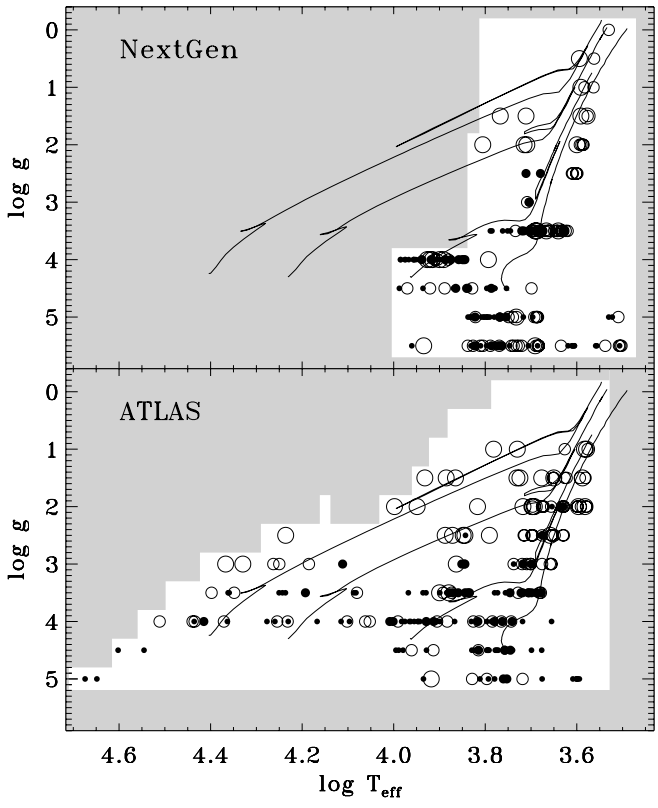

FIG. 11.—The $\log T_{\rm eff}$ vs. $\log g$ distribution of ATLAS and NextGen fitting output for GS83 and JHC84 stars. Luminosity classes: *small filled circles*, MK V; *large filled circles*, IV; *small open circles*, III; *large open circles*, II–I. The evolutionary tracks for stars of solar metallicity and $M = 1$, 2, and 5 $M_{\odot}$ from Girardi et al. (2000) and for 10 $M_{\odot}$ from Salasnich et al. (2000) are also superposed. The white region shows the parameter space covered by the theoretical libraries (see also Fig. 1).

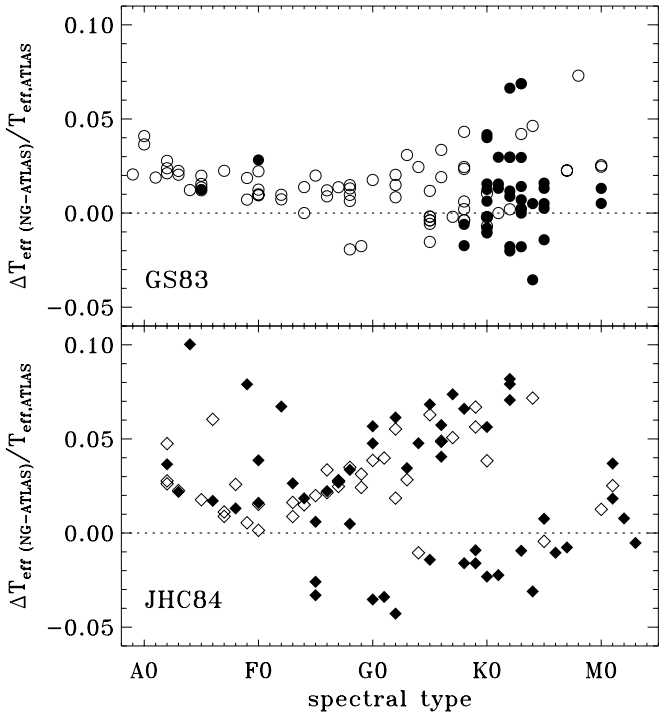

FIG. 12.—Temperature residuals for the 216 GS83 (*top*) and JHC84 stars (*bottom*) with both ATLAS and NextGen best-fit solution. Stars are labeled according to their MK luminosity class (MK IV–V, *open markers*; MK I–III, *filled markers*). Note, in the JHC84 plot, the peculiar distribution of giant stars along two distinct point sequences. Over the whole sample, NextGen tends to predict, on average, an effective temperature about 2% warmer than the ATLAS value (see text for a full discussion of these two important features).

electronic pressure and a cooler temperature profile versus. stellar spatial coordinate (i.e., radius or optical depth, cf. e.g., Scholz & Tsuji 1984). To some extent, this is the physical consequence of the gravity decreasing outward in the stellar photosphere; with a lower gravity, in fact, thermodynamical equilibrium in the external layers readjusts so as to allow a lower pressure of the electronic plasma (because of an increased mean distance between atoms and a higher dumping potential for the bound-bound and bound-free e^- transitions) and a cooler temperature, still sufficient, however, to "sustain" the atmospheric structure.

As a result, for fixed $T_{\rm eff}$ and $\log g$, the SED of a "spherical" star is therefore expected to display sharper absorption lines and a "redder" continuum. Among other effects, this should also result in a less severe blanketing absorption (see Hauschildt et al. 1999b) as a consequence of a reduced blend of metal absorption lines at short wavelengths.

A second related effect that should be dealt with, when comparing plane-parallel and spherical model atmospheres, is limb darkening. Because of the geometry, in fact, the integrated flux that emerges from a "spherical" star receives a more important contribution from low-gravity cooler layers and therefore appears, on average, "cooler" with respect to its corresponding plane-parallel model (Claret & Hauschildt 2003).

This feature also emerges from the recent results of Fields et al. (2003) on the microlensing surface scanning of the K3 giant star related to the EROS BLG2000-5 event. Surface brightness measurements for this star are, in fact, inconsistent with the NextGen best-fit predictions at higher than 10 σ and indicate that the derived $T(\tau)$ vertical structure of

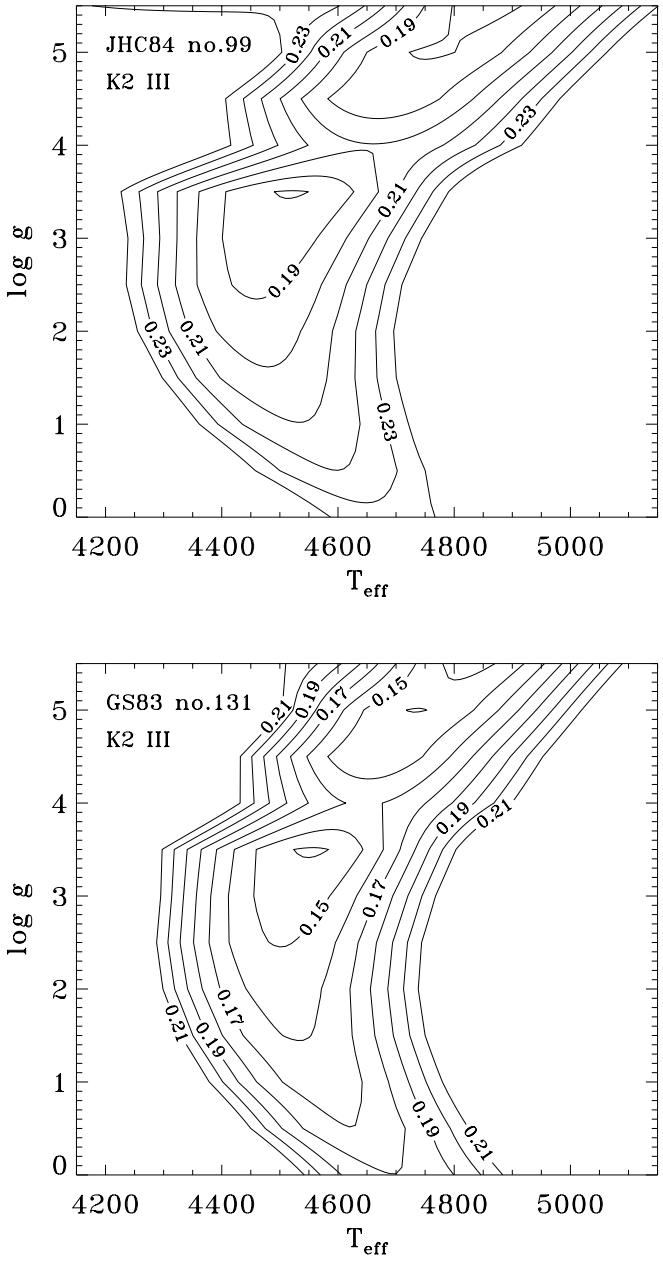

FIG. 13.—Illustrative example of the NextGen fitting procedure for two K2 giant stars from the GS83 and JHC84 samples. Plotted is the map of the standard deviation, *s*, of residual flux between observed and theoretical SED across the model grid (according to eq. [4]) in the $T_{\rm eff}$ vs. log *g* phase space. One sees that two best-fit solutions can be identified in each plot, one correctly placing the K2 III stars in the low-temperature low-gravity region (i.e., $T_{\rm eff} \sim 4500$ K, $\log g \sim 3.0$ dex) and the other *nominally better* one shifting stars to slightly warmer temperature and much higher gravity ($T_{\rm eff} \sim 4800$ K, $\log g \sim 5.5$ dex).

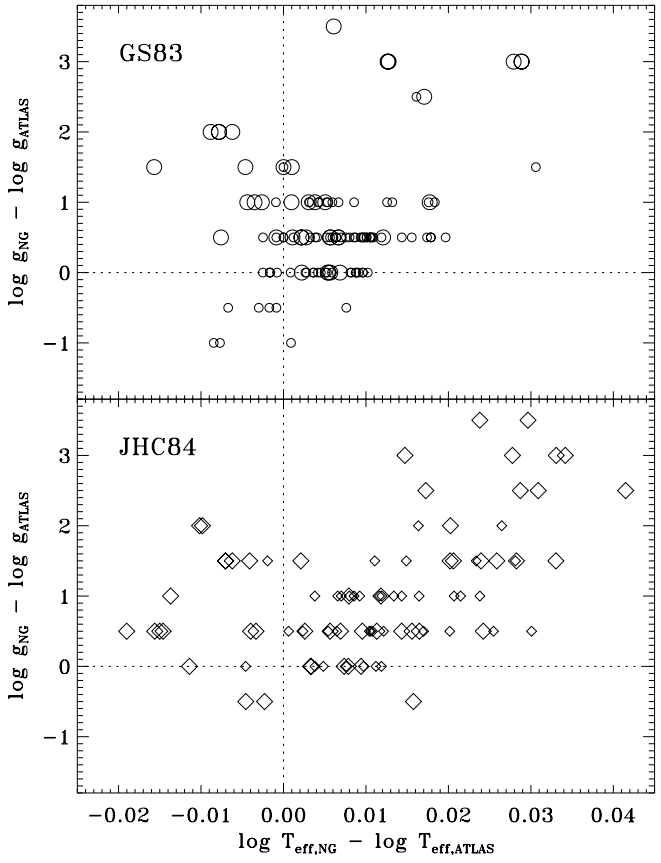

FIG. 14.—Temperature and gravity difference between ATLAS and NextGen best-fit solutions for 216 stars in the GS83 and JHC84 samples. Marker size is proportional to the MK luminosity class (i.e., *large symbols*, MK I–III giants; *small symbols*, MK IV–V dwarfs). A correlation between $\Delta T_{\rm eff}$ and $\Delta \log g$, especially for giant stars in the JHC84 plot, is evident.

the theoretical atmosphere noticeably overestimates limb-darkening effects.

6. SUMMARY AND CONCLUSIONS

In this work we carried out a combined comparison of the two theoretical codes ATLAS (Kurucz 1992b) and NextGen (Hauschildt et al. 1999a, 1999b) for stellar atmosphere synthesis. Our tests relied on the fit of a set 334 target stars of nearly solar metallicity, spanning the whole sequence of spectral types and luminosity class, observed in the optical range by Gunn & Stryker (1983) and Jacoby et al. (1984).

For about 80% of this sample we obtained an estimate of the physical parameters ($T_{\rm eff}$, $\log g$) of stars and their related statistical uncertainty by means of an original fitting procedure that matched the observed SED with the ATLAS and NextGen model grids.

This provided a twofold application of our results; on one hand, we achieved a self-consistent and independent calibration of the temperature and bolometric scale for giant and dwarf stars versus empirical classification parameters (i.e., spectral type and MK luminosity class). On the other hand, the comparison of the synthetic templates from the ATLAS and NextGen model grids allowed us to directly assess the relative performances of each theoretical code so as to reproduce SEDs of real stars according to the different input physics adopted.

The comparison of our results with several empirical calibration scales in the literature (see § 4) led to the following main conclusions:

1. The good fitting accuracy ($\sigma_{\rm flux} \sim 2\%-5\%$) of both theoretical models in reproducing SEDs of early-type stars (spectral type F and earlier) drastically degrades at lower $T_{\rm eff}$, especially for K stars in which both ATLAS and NextGen codes still fail to properly account for the increasing contribution of molecular features in the spectra of stars. In general, ATLAS is found to provide a systematically better fit (a factor of 2 lower residual $\sigma_{\rm flux}$) than NextGen along the whole B → K spectral-type sequence, although the NextGen grid, because of its lower $T_{\rm eff}$ limit, more efficiently matches M stars.

2. Comparing with empirical calibrations, both ATLAS and NextGen tend, on average, to predict warmer (by 4%–8%) $T_{\rm eff}$ for both giant and dwarf stars of fixed spectral type. As for the ATLAS models, this effect has probably much to do with the imperfect treatment of metal blanketing at short wavelengths (as extensively discussed, for instance, by Castelli et al. 1997), while the case of NextGen seems more entangled.

This issue has been further explored in § 5 by comparing the ATLAS versus NextGen template sequences for 216 stars in the GS83 and JHC84 catalogs with nominal best fit in the $3500 \leq T_{\rm eff} \leq 10,000$ K temperature range. As a general feature, NextGen best-fit solutions are found to predict a temperature and gravity higher than the corresponding ATLAS solutions for given target stars. The effect is especially evident for MK I–III objects, for which the NextGen fails to correctly settle $\log g$ and noticeably overestimates surface gravity in about 25% of the cases versus 4% for ATLAS. This misclassification partly derives from the lesser capability of NextGen spherical models to reproduce the SED of giant stars, compared to the fit with the plane-parallel geometry. In most cases the latter proved in fact to be formally more accurate, leading however to a less physical combination of the fundamental parameters of stars.

An in-depth analysis of the fit accuracy for SED of target stars shows that, to some extent, the NextGen $T_{\rm eff}$ and $\log g$ excess is correlated, as a consequence of a sort of "degeneracy" in the solution space (Buzzoni et al. 2001). The effect is likely magnified in our framework when considering that, for low-gravity stars, ATLAS model atmospheres assume standard plane-parallel layers while NextGen adopts a spherical-shell geometry. Because of a more important contribution of external atmosphere layers to the integrated emerging flux in the case of the NextGen output, for fixed $T_{\rm eff}$ and $\log g$ this implicitly calls for a "redder" theoretical SED and a reduced blanketing absorption of metal blends at short wavelengths, as a consequence of "sharper" spectral features.

The possible overestimate of the limb-darkening effects, as a consequence of the adopted $T(\tau)$ vertical structure of NextGen model atmospheres, seems also a critical issue in this regard, as indicated by the recent observations of the EROS BLG2000-5 microlensing event.

It is a pleasure to thank the anonymous referee for his/her competent suggestions that greatly helped in refining some important issues of our discussion.

This work received partial financial support from the Italian MURST under grant COFIN00 02-016 and from the Mexican CONACyT via grant 36547-E. This research has made use of the SIMBAD database, operated at CDS, Strasbourg, France.

REFERENCES

Adelman, S. J. 1999, MNRAS, 310, 146
Allard, F., Hauschildt, P. H., & Schweitzer, A. 2000, ApJ, 539, 366
Alonso, A., Arribas, S., & Martínez-Roger, C. 1999, A&AS, 140, 261
Anders, E., & Grevesse, N. 1989, Geochim. Cosmochim. Acta, 53, 197
Andrievsky, S. M., et al. 2002, A&A, 381, 32
Bartasiute, S., Ezhkova, O. V., & Lazauskaite, R. 1999, Baltic Astron., 8, 465
Bartkevicius, A., & Lazauskaite, R. 1996, Baltic Astron., 5, 1
———. 1997, Baltic Astron., 6, 499
Bertone, E. 2001, Ph.D. thesis, Università di Milano
Bertone, E., & Buzzoni, A. 2001, in First *COROT*/*MONS*/*MOST* Ground-based Support Workshop, ed. C. Sterken (Brussels: Vrije Univ. Brussel), 75
Bessell, M. S. 1990, PASP, 102, 1181
———. 1991, AJ, 101, 662
Bessell, M. S., Castelli, F., & Plez, B. 1998, A&A, 333, 231
Böhm-Vitense, E. 1958, Z. Astrophys., 46, 108
———. 1981, ARA&A, 19, 295
Bruzual, A. G., & Charlot, S. 1993, ApJ, 405, 538
Burkhart, C., & Coupry, M. F., 1998, A&A, 338, 1073
Buzzoni, A., Chavez, M., Malagnini, M. L., & Morossi, C. 2001, PASP, 113, 1365
Castelli, F., Gratton, R. G., & Kurucz, R. L. 1997, A&A, 318, 841
Cayrel de Strobel, G., Soubiran, C., Friel, E. D., Ralite, N., & François, P. 1997, A&AS, 124, 299
Cayrel de Strobel, G., Soubiran, C., & Ralite, N. 2001, A&A, 373, 159
Cenarro, A. J., Cardiel, N., Gorgas, J., Peletier, R. F., Vazdekis, A., & Prada, F. 2001, MNRAS, 326, 959
Claret, A., & Hauschildt, P. H. 2003, A&A, 412, 241
Claria, J. J., Piatti, A. E., & Osborn, W. 1996, PASP, 108, 672
Code, A. D., Davies, J., Bless, R. C., & Hanbury Brown, R. 1976, ApJ, 203, 417
Di Benedetto, G. P. 1998, A&A, 339, 858
Edvardsson, B., Andersen, J., Gustafsson, B., Lambert, D. L., Nissen, P. E., & Tomkin, J. 1993, A&A, 275, 101
Eggen, O. J. 1991, AJ, 102, 1826
———. 1998, AJ, 115, 2397
Faber, S. M., Friel, E. D., Burstein, D., & Gaskell, C. M. 1985, ApJS, 57, 711
Fanelli, M. N., O'Connell, R. W., & Thuan, T. X. 1987, ApJ, 321, 768
Fields, D. L., et al. 2003, ApJ, 596, 1305
Flower, P. J. 1977, A&A, 54, 31
Flynn, C., & Morell, O. 1997, MNRAS, 286, 617
Friel, E. D., & Janes, K. A. 1993, A&A, 267, 75
Fry, A. M., & Carney, B. W. 1997, AJ, 113, 1073
Geisler, D., Claria, J. J., & Minniti, D. 1991, AJ, 102, 1836
Girardi, L., Bressan, A., Bertelli, G., & Chiosi, C. 2000, A&AS, 141, 371
Gray, R. O., Graham, P. W., & Hoyt, S. R. 2001, AJ, 121, 2159
Guiderdoni, B., & Rocca-Volmerange, B. 1987, A&A, 186, 1
Gunn, J. E., & Stryker, L. L. 1983, ApJS, 52, 121 (GS83)
Gustafsson, B., Bell, R. A., Eriksson, K., & Nordlund, Å. 1975, A&A, 42, 407
Gustafsson, B., Edvardsson, B., Eriksson, K., Mizuno-Wiedner, M., Jörgensen, U. G., & Plez, B. 2003, in ASP Conf. Ser. 288, Stellar Atmosphere Modeling, ed. I. Hubeny, D. Mihalas, & K. Werner (San Francisco: ASP), 331
Hartkopf, W. I., & Yoss, K. M. 1982, AJ, 87, 1679
Hauschildt, P. H., Allard, F., & Baron, E. 1999a, ApJ, 512, 377
Hauschildt, P. H., Allard, F., Ferguson, J., Baron, E., & Alexander, D. R. 1999b, ApJ, 525, 871
Hauschildt, P. H., Baron, E., Starrfield, S., & Allard, F. 1996, ApJ, 462, 386
Haywood, M. 2001, MNRAS, 325, 1365
Holweger, H. 1970, A&A, 4, 11
Jacoby, G. H., Hunter, D. A., & Christian, C. A. 1984, ApJS, 56, 257 (JHC84)
Jaschek, C., & Jaschek, M. 1995, The Behaviour of Chemical Elements in Stars (Cambridge: Cambridge Univ. Press)
Johnson, H. L. 1966, ARA&A, 4, 193
Kjaergaard, P. 1984, A&AS, 56, 313
Knude, J. 1989, A&AS, 81, 215
Kurucz, R. L. 1970, SAO Spec. Rep., No. 309
———. 1979, ApJS, 40, 1
———. 1992a, Rev. Mexicana Astron. Astrofis., 23, 45
———. 1992b, in IAU Symp. 149, The Stellar Populations of Galaxies, ed. B. Barbuy & A. Renzini (Dordrecht: Kluwer), 225
———. 1995, Kurucz CD-ROM 13, ATLAS9 Stellar Atmosphere Programs and 2 km/s Grid (Cambridge: SAO), revised
Laird, J. B., Carney, B. W., & Latham, D. W. 1988, AJ, 95, 1843
Lambert, D. L., Gustafsson, B., Eriksson, K., & Hinkle, K. H. 1986, ApJS, 62, 373
Luck, R. E. 1982, ApJ, 263, 215
Luck, R. E., & Bond, H. E. 1989, ApJS, 71, 559
Norris, J. 1986, ApJS, 61, 667
Perrin, G., Coudé Du Foresto, V., Ridgway, S. T., Mariotti, J.-M., Traub, W. A., & Carleton, N. P. 1998, A&A, 331, 619
Pickles, A. J. 1985, ApJS, 59, 33
Plez, B. 1990, Mem. Soc. Astron. Italiana, 61, 765
Plez, B., Brett, J. M, & Nordlund, Å. 1992, A&A, 256, 551
Ridgway, S. T., Joyce, R. R., White, N. M., & Wing, R. F. 1980, ApJ, 235, 126
Salasnich, B., Girardi, L., Weiss, A., & Chiosi, C. 2000, A&A, 361, 1023
Schiavon, R. P., Barbuy, B., & Singh, P. D. 1997, ApJ, 484, 499
Scholz, M., & Tsuji, T. 1984, A&A, 130, 11
Strom, S. E., & Kurucz, R. L. 1966, J. Quant. Spectrosc. Radiat. Transfer, 6, 591

Takeda, Y., & Takada-Hidai, M. 1998, PASJ, 50, 629
Taylor, B. J. 1991, ApJS, 76, 715
———. 1999, A&AS, 134, 523
Thogersen, E. N., Friel, E. D., & Fallon, B. V., 1993, PASP, 105, 1253
Tsuji, T. 1976, PASJ, 28, 543
Venn, K. A., Brooks, A. M., Lambert, D. L., Lemke, M., Langer, N., Lennon, D. J., & Keenan, F. P. 2002, ApJ, 565, 571
Wesselink, A. J. 1969, MNRAS, 144, 297
Worthey, G., Faber, S. M., Gonzalez, J. J., & Burstein, D. 1994, ApJS, 94, 687
Xu, Z. 1991, A&A, 248, 367
Zakhozhaj, V. A., & Shaparenko, E. F. 1996, Kinematika Fiz. Nebesn. Tel., 12, 20